# A DFT Study of the Hydrogen Storage Potentials and Properties of Ca, Fe, and Ti Deposited NaSi$_{20}$ Fullerenes

Huixi Yang[1], Bin Liu[1*], Hongjiang Ren[2*]

[1]Xi'an Key Laboratory of Textile Chemical Engineering Auxiliaries, School of Environmental and Chemical Engineering, Xi'an Polytechnic University, Xi'an 710600, PR China.
[2]School of Chemical Engineering, Xi'an University, Xi'an 710065, PR China.

*Corresponding author:* Bin Liu; Hongjiang Ren, email: hjren@xawl.edu.cn

**Abstract.** In this work, the hydrogen storage materials of Ca, Fe, and Ti deposited NaSi$_{20}$ clusters were investigated utilizing DFT methods (B3LYP and M06-2X) combined with the 6-311++G(*d*, *p*) basis set. The results show that Ca, Fe, and Ti atoms tend to bind with two adjacent Si atoms. The Ca@NaSi$_{20}$, Fe@NaSi$_{20}$, and Ti@NaSi$_{20}$ can adsorb up to three, four, and six hydrogen molecules, respectively. The adsorption energy ($E_{ads}$) per hydrogen molecule meets the United States Department of Energy (DOE) target for hydrogen storage materials for $n$H$_2$-Ti@NaSi$_{20}$ ($n$ = 2-6) and $n$H$_2$-Fe@NaSi$_{20}$ ($n$ = 1- 4), implying that NaSi$_{20}$ fullerene could be a potentially suitable material for hydrogen storage.
**Keywords:** NaSi$_{20}$ fullerenes; DFT methods; hydrogen storage.

**Resumen.** Utilizando métodos de la DFT (B3LYP y M06-2X) combinados con las bases 6-311++G(*d*, *p*), en este trabajo se investigaron materiales para el almacenamiento de hidrógeno a base de Ca, Fe, y Ti depositados en cúmulos de NaSi$_{20}$. Los resultados muestran que los átomos de Ca, Fe, y Ti tienden a unirse a dos átomos adyacentes de Si. Los cúmulos Ca@NaSi$_{20}$, Fe@NaSi$_{20}$, y Ti@NaSi$_{20}$ pueden adsorber hasta tres, cuatro y seis moléculas de hidrógeno, respectivamente. Las energías de adsorción por molécula de hidrógeno ($E_{ads}$) de $n$H$_2$-Ti@NaSi$_{20}$ ($n$ = 2-6) y $n$H$_2$-Fe@NaSi$_{20}$ ($n$ = 1- 4) cumplen con el objetivo del Departamento de Energía de los Estados Unidos (DOE) lo que implica que el fullereno NaSi$_{20}$ puede ser un material potencialmente adecuado para el almacenamiento de hidrógeno.
**Palabras clave:** NaSi$_{20}$ fullerenos; métodos de la DFT; almacenamiento de hidrógeno.

## Introduction

With the growth of the world population and rapid economic development, as well as the shortage of fossil fuels and global environmental problems that threaten the peaceful existence of mankind and stimulate people's determination to find new energy sources [1,2]. Hydrogen as a renewable and clean energy source has several ideal characteristics, for example, it contains the maximum energy per unit weight, is abundant in the natural environment, and its combustion products do not pollute the environment like sulfur oxidation and aromatic hydrocarbon oxides [3,4]. The U. S. Department of Energy (DOE) system has identified goals for hydrogen storage materials, the average adsorption energy per H$_2$ (average adsorption energy per H$_2$, $E_{ad}$/H$_2$) in

an ideal hydrogen storage material should be between chemisorption and physical adsorption (0.1 - 0.8 eV) to meet the hydrogen storage reversibility of the material [5].

Currently, there are many types of hydrogen storage materials. Carbon-based and chemically active hydrogen storage materials include fullerene, graphene, carbon nanotubes, etc [6,7]. Nano-structured magnesium and magnesium-based hydrides can also be used to store hydrogen through adsorption [8]. In recent years, the semiconductor cluster has become one of the research objects in cluster science and the silicon cluster is the most widely used technology in the semiconductor cluster [9-13].

Silicon is not only rich in content but is also one of the most important materials in the modern industry [11-13]. It has a wide range of applications in various areas of life, such as metallurgy, electronic manufacturing, the military industry, medical, etc [10-12]. But at the same time, the disadvantages of silicon materials are also very obvious. For example, the hollow structure of silicon and the lack of unsaturated bonds in silicon valence electrons with $sp^2$ hybridization deliver unstable fullerene cages (silicon nanotubes and silicon fullerenes) [10]. However, studies over the years have shown that their structures can be improved by various chemical modifications, such as encapsulating metal atoms in clusters [11] or using H adsorption to enhance the $sp^3$ bonding between Si atoms to improve stability [12]. Meanwhile, Ryou *et al.* found that the binding energy of hydrogen molecules to silicon nanotubes is less than 0.1 eV even in stable structures through DFT calculations, and then pure silicon nanotubes are not suitable for hydrogen storage [13]. Kumar *et al.* found that metal doping enhanced the stability and size selectivity of silicon clusters [14]. Sporea *et al.* stabilized silicon clusters by encapsulating alkali metal atoms Na, K, and Li inside $Si_{20}$, which can provide regular shapes for $Si_{20}$ clusters [15]. Moreover, Ammar *et al.* investigated the hydrogen storage properties of $KSi_{20}$ and $Ti@KSi_{20}$ using the DFT-based B3YLP and M06-2X methods. The adsorption energy values ($\bar{E}_{ads}$) per hydrogen molecule satisfy the U.S. DOE targets for hydrogen storage materials [16].

According to our knowledge, $NaSi_{20}$ should have similar hydrogen storage properties to $KSi_{20}$. However, the hydrogen storage performance of $NaSi_{20}$ has not been reported. And more importantly, as previously reported by researchers, Ca, Fe, and Ti metal atoms were often considered and performed well in the previous studies of modified carbon-based and boron-based hydrogen storage materials [17-19]. Meanwhile, Ca is one of the most active atoms in alkaline earth metals, Fe is the transition metal atom with more outer electrons, and Ti is the transition metal atom with fewer outer electrons. To the best of our knowledge, $NaSi_{20}$ deposited with Ca, Fe, and Ti atoms has not been previously investigated as hydrogen storage materials. In this work, the storage characteristics of $H_2$ on Na-encapsulated $Si_{20}$ ($NaSi_{20}$) clusters deposited in Ca, Fe, and Ti were investigated by performing DFT calculations at the theoretical level of B3LYP and M06-2X combined with the 6-311++G($d, p$) basis set. The effect of electron properties on $NaSi_{20}$ fullerenes deposited in Ti, Ca, and Fe was studied. Then the adsorption of *n* hydrogen molecules (*n* = 1-6) on $Ca@NaSi_{20}$, $Fe@NaSi_{20}$, and $Ti@NaSi_{20}$ is discussed.

## Computational methods

To investigate the storage properties of $H_2$ molecules on $Ca@NaSi_{20}$, $Fe@NaSi_{20}$, and $Ti@NaSi_{20}$ fullerenes, DFT calculations [20] were performed at the B3LYP/6-311++G($d, p$) and M06-2X/6-311++G($d, p$) levels of theory for the non-metallic atoms (H, Si) and an effective for the effective pseudopotential basis set LANL2DZ of Na, Ca, Fe and Ti atoms, respectively [20]. Full geometric optimizations were carried out at two levels for free $H_2$ molecules, $Si_{20}$, $NaSi_{20}$, $Ca@NaSi_{20}$, $Fe@NaSi_{20}$, and $Ti@NaSi_{20}$ substrates as well as $nH_2$-$Ca@NaSi_{20}$ (*n* = 1-3), $nH_2$-$Fe@NaSi_{20}$ (*n* = 1-4), and $nH_2$-$Ti@NaSi_{20}$ (*n* = 1-6) complexes. Because silicon is the most readily available semiconductor in nature, hydrogen can be adsorbed on silicon in both crystalline and amorphous forms and can be desorbed again. Several experimental and theoretical studies have been conducted by Mao WL and Mao HK to investigate whether porous silicon is capable of conducting hydrogen storage [21]. All the calculations were calculated using the Gaussian 09 program [22].

The ionization potential (IP), electron affinity (EA), and chemical hardness (η) can be expressed in equations 1-3, where E(N-1), E(N), and E(N+1) are total energies when the system has N-1, N and N+1 electrons, respectively.

$$IP = E(N-1) - E(N) \tag{1}$$

$$EA = E(N) - E(N+1) \tag{2}$$

$$\eta \approx \frac{1}{2}\left(IP\text{-}EA\right) \tag{3}$$

The average binding energy $(\overline{E}_b)$ of per atom for $Si_{20}$, $NaSi_{20}$, $Ca@NaSi_{20}$, $Fe@NaSi_{20}$, and $Ti@NaSi_{20}$ is calculated by equation (4),

$$\overline{E}_b = \frac{E_{cluster} - \sum E_{atom}}{n} \tag{4}$$

where Ecluster is the energy of the optimized cluster, $\sum E_{atom}$ is the sum of the energies of the free atoms of the cluster and n is total number of the cluster atoms. The binding energies ($E_{bind}$) of Ca, Fe, and Ti atoms on $NaSi_{20}$ substrate clusters are calculated by equation (5). $nH_2$ molecule ($n$ = 1-6) adsorption energies ($E_{ads}$) and the average adsorption energy of per hydrogen molecule ($\overline{E}_{ads}$) on $M@NaSi_{20}$ fullerenes (M = Ca, Fe and Ti) are calculated by equations (6) and (7), respectively.

$$E_{bind} = E_{M@NaSi_{20}} - (E_{NaSi_{20}} + E_M) \tag{5}$$

$$E_{ads} = E_{nH_2\text{-}M@NaSi_{20}} - (nE_{H_2} + E_{M@NaSi_{20}}) \tag{6}$$

$$\overline{E}_{ads} = \frac{1}{n}[E_{nH_2\text{-}M@NaSi_{20}} - (nE_{H_2} + E_{M@NaSi_{20}})] \tag{7}$$

where $E_{M@NaSi_{20}}$ is the energy of the optimized $Ca@NaSi_{20}$, $Fe@NaSi_{20}$, and $Ti@NaSi_{20}$ complexes, $E_{M@NaSi_{20}}$ is the energy of the corresponding optimized $NaSi_{20}$ substrate clusters, $E_M$ is the atomic energy of the free M (M = Ca, Fe, and Ti) atoms, and $E_{nH_2\text{-}M@NaSi_{20}}$ is the total energy of the optimized $nH_2$-$M@NaSi_{20}$ (M = Ca, Fe, and Ti).

The enthalpy difference ($\Delta H^{\Theta}$) and free energy difference ($\Delta G^{\Theta}$) of $nH_2$-$M@NaSi_{20}$ (M = Ca, Fe, and Ti) complexes are calculated by equations (8) and (9), respectively [23].

$$\Delta H^{\Theta} = \left[ H^{\Theta}_{nH_2\text{-}M@NaSi_{20}} - \left( nH^{\Theta}_{H_2} + H^{\Theta}_{M@NaSi_{20}} \right) \right]/n \tag{8}$$

where, $H^{\Theta}_{nH_2\text{-}M@NaSi_{20}}$, $H^{\Theta}_{M@NaSi_{20}}$, and $H^{\Theta}_{H_2}$ are the enthalpies for $nH_2$-$M@NaSi_{20}$, $M@NaSi_{20}$ and $H_2$ molecules, respectively.

$$\Delta G^{\Theta} = \left[ G^{\Theta}_{nH_2\text{-}M@NaSi_{20}} - \left( nG^{\Theta}_{H_2} + G^{\Theta}_{M@NaSi_{20}} \right) \right]/n \tag{9}$$

where $G^{\Theta}_{nH_2\text{-}M@NaSi_{20}}$, $G^{\Theta}_{M@NaSi_{20}}$ and $G^{\Theta}_{H_2}$ are the free energies of $nH_2$-$M@NaSi_{20}$, $M@NaSi_{20}$, and $H_2$ molecules, respectively.

For testing the stability of the wave function of our investigated systems, the keywords of UB3LYP, stable and nosymm are used in the examples for both $4H_2/Ti@NaSi20$ and $4H_2/Fe@NaSi20$ complexes and the results show that the wave functions are stable under the perturbations considered. The corresponding figure is given in Supplement 1.

## Results and discussion

### Geometric structure and electronic properties of Ca@NaSi$_{20}$, Fe@NaSi$_{20}$, and Ti@NaSi$_{20}$ clusters

Fig. 1 shows the optimized structures of $Si_{20}$ and $NaSi_{20}$ fullerenes, as well as Ca, Fe, and Ti external doping $NaSi_{20}$ fullerenes, named Ca@NaSi$_{20}$, Fe@NaSi$_{20}$, and Ti@NaSi$_{20}$ clusters. The geometrical and electronic properties of the investigated clusters are listed in Table 1. As can be seen from Fig. 1**(a)**, the $Si_{20}$ fullerene cluster is a distorted cage with the shortest Si-Si bond length ($d_{Si-Si}$) of 2.279 Å and dipole moments of 1.198 Debye at the B3LYP level, and the shortest Si-Si bond length ($d_{Si-Si}$) of 2.291 Å and dipole moments of 1.215 Debye at the M06-2X level. This is similar to the value of Si-Si bond length ($d_{Si-Si}$) calculated by Ammar *et al.*, which is 2.335 Å for Si-Si bond length ($d_{Si-Si}$) calculated by B3LYP method and 2.381 Å for Si-Si bond length ($d_{Si-Si}$) calculated by M06-2X method. After a Na atom is embedded in the $Si_{20}$ cluster, the structure of the cluster has changed into a regular shape, as shown in Fig. 1**(b)**. Compared with pure silicon clusters without internally doped metal atoms, the shape of $NaSi_{20}$ clusters is more uniform. Under the B3LYP method, the Si-Si bond length ($d_{Si-Si}$) is reduced to 2.777 Å, which is similar to the results previously reported by Borshch et al. [24]. The HOMO-LUMO gap ($E_g$) decreased from 2.163 and 3.486 eV to 1.329 and 2.512 eV, respectively. Chemical hardness ($\eta$) decreased by 38.63 % and 27.94 %, respectively, while the average binding energy between atoms ($\overline{E}_b$) increased by 4.5 % and 5.2 %.

**Table 1.** Ionization potential (IP, eV), electron affinity (EA, eV), hardness ($\eta$, eV), HOMO and LUMO energy gap ($E_g$, eV), binding energy per atom ($E_b$, eV), dipole moment (D, Debye), bond length (d, Å), binding energy ($E_{bind}$, eV) of $Si_{20}$, $NaSi_{20}$, Ca@NaSi$_{20}$, Fe@NaSi$_{20}$ and Ti@NaSi$_{20}$ as well as Mulliken charges ($Q_M$, e) of Ca, Fe, Ti atoms in the clusters.

| | Si$_{20}$ | | NaSi$_{20}$ | | Ca@NaSi$_{20}$ | | Fe@NaSi$_{20}$ | | Ti@NaSi$_{20}$ | |
|---|---|---|---|---|---|---|---|---|---|---|
| | **B3LYP** | **M06-2X** | **B3LYP** | **M06-2X** | **B3LYP** | **M06-2X** | **B3LYP** | **M06-2X** | **B3LYP** | **M06-2X** |
| **IP** | 5.780 | 6.581 | 5.255 | 5.922 | 4.761 | 5.485 | 5.372 | 5.656 | 5.209 | 5.391 |
| **EA** | 3.616 | 3.095 | 3.926 | 3.410 | 3.776 | 3.303 | 3.911 | 3.831 | 3.795 | 3.432 |
| **$\eta$** | 1.082 | 1.743 | 0.664 | 1.256 | 0.493 | 1.091 | 0.730 | 0.913 | 0.707 | 0.979 |
| **$E_g$** | 2.163 | 3.486 | 1.329 | 2.512 | 0.986 | 2.182 | 1.460 | 1.825 | 1.414 | 1.959 |
| **$E_b$** | -4.285 | -4.540 | -4.091 | -4.306 | -3.955 | -4.155 | -4.137 | -4.286 | -4.103 | -4.250 |
| **D** | 1.198 | 1.215 | 0.163 | 0.259 | 11.843 | 11.489 | 2.966 | 1.597 | 8.502 | 9.983 |
| **$d_{Si-Si}/d_{M-Si}$** | 2.279 | - | 2.777 | - | 3.013 | - | 2.367 | - | 2.502 | - |
| **$E_{bind}$** | | | | | -1.091 | -0.992 | -5.109 | -3.877 | -4.348 | -3.069 |
| **$Q_M$** | | | | | 1.266 | 1.042 | -0.184 | -0.123 | 0.398 | 0.466 |

We studied the external doping of Ca, Fe, and Ti atoms at different positions of $NaSi_{20}$ fullerene. The structure with the most stable energy after optimization is shown in Fig. 1. The results show that Ca, Fe, and Ti

are bound to the $NaSi_{20}$ cluster by bonding with two adjacent silicon atoms, which is the same as the external doping mode of Ti atoms to the $KSi_{20}$ cluster in the cluster studied by Ammar et al. [14].

According to Baei's theory, the size of the energy gap ($E_g$)value is closely related to the activity and stability of chemical reactions [25]. Under the density functional B3LYP method, the energy gap ($E_g$) of the $NaSi_{20}$ cluster modified by Fe and Ti atoms is larger than that of the $NaSi_{20}$ cluster modified by Ca atoms, while the energy gap ($E_g$) of the $NaSi_{20}$ cluster modified by Ca atoms is smaller than that of the $NaSi_{20}$ cluster. Similarly, with the B3LYP method, the chemical hardness ($\eta$) of the $Fe@NaSi_{20}$ cluster and $Ti@NaSi_{20}$ cluster increases by 9.93 % and 6.48 %, respectively, while the chemical hardness ($\eta$) of the $Ca@NaSi_{20}$ cluster decreases by 25.75 %. With the M06-2X method, the $Ca@NaSi_{20}$, $Fe@NaSi_{20}$, and $Ti@NaSi_{20}$ clusters have smaller energy gaps than the $NaSi_{20}$ clusters. The $Ca@NaSi_{20}$, $Fe@NaSi_{20}$, and $Ti@NaSi_{20}$ clusters also have smaller $\eta$ values than the $NaSi_{20}$ clusters. Under the M06-2X method, $\eta$ values of $Ca@NaSi_{20}$, $Fe@NaSi_{20}$ and $Ti@NaSi_{20}$ are reduced by 22.05 %, 27.31 % and 13.14%, respectively. Since the density functional M06-2X method considers the weak interaction, it can well describe the weak interaction between metals and clusters. At the same time, the M06-2X method is effective in calculating the energy of the reactants, the isomerization process and the reaction energy barrier. The results showed that the chemical reactivity of $Ca@NaSi_{20}$, $Fe@NaSi_{20}$, and $Ti@NaSi_{20}$ clusters was better than that of $NaSi_{20}$ clusters. Compared with $NaSi_{20}$ clusters, the average binding energy ($\overline{E}_b$) of $NaSi_{20}$ clusters modified by Ca, Fe, and Ti atoms increases by about 3.51 %, 0.47 %, and 1.31 %, respectively, under M06-2X method. However, the average binding energy ($\overline{E}_b$) of $NaSi_{20}$ clusters modified by Fe and Ti atoms calculated by the B3LYP method decreases by 1.12 % and 1.20 %, respectively, and for $Ca@NaSi_{20}$, the mean binding energy ($\overline{E}_b$) increases by about 3.61 %. This is consistent with the changing trend of the binding energy of $C_{20}$ and $KSi_{20}$ clusters modified by Ti atoms reported by Ammar et al. [12]. It can be seen that the external doping of Ca, Fe and Ti atoms on the $NaSi_{20}$ cluster reduces the stability of $NaSi_{20}$ and increases the activity of the reaction.
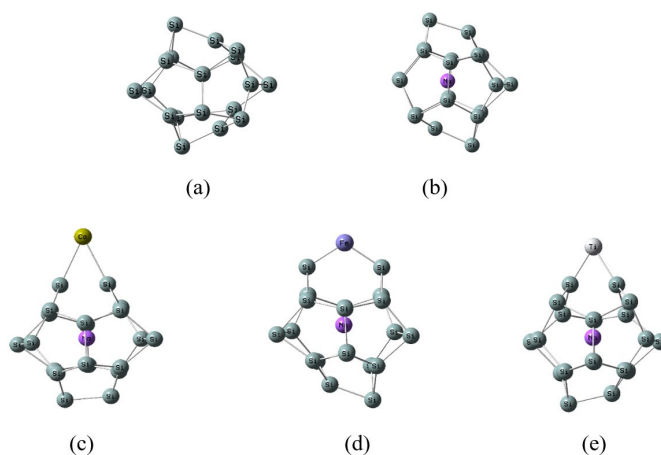


**Fig. 1.** The optimized structures of **(a)** $Si_{20}$, **(b)** $NaSi_{20}$, **(c)** $Ca@NaSi_{20}$, **(d)** $Fe@NaSi_{20}$ and **(e)** $Ti@NaSi_{20}$ calculated at B3LYP method.

## Interaction of $H_2$ on $Ca@NaSi_{20}$, $Fe@NaSi_{20}$, and $Ti@NaSi_{20}$

In this work, hydrogen molecules are stored on optimized $Ca@NaSi_{20}$, $Fe@NaSi_{20}$, and $Ti@NaSi_{20}$ clusters to characterize the properties of the selected hydrogen storage materials. Fig. 2 shows the geometry of $nH_2$-$Ca@NaSi_{20}$, $nH_2$-$Fe@NaSi_{20}$, and $nH_2$-$Ti@NaSi_{20}$ clusters and in order to explore the place of adsorption more clearly, the structure diagrams from different viewpoints for $4H_2$-$Fe@NaSi_2$ and $6H_2$-$Ti@NaSi_{20}$ as well as different direction of hydrogen attacking for $Ti@NaSi_{20}$ and $Fe@NaSi_{20}$ are given in Fig. 3. As can be seen from Fig. 2, the H-H bonds of all $H_2$ molecules are not broken, and they are all adsorbed by metal atoms in the form of molecules. Parameters such as dipole moment, bond length and Mulliken charge of adsorbed clusters are shown

in Tables 2-4, respectively. Equations (6) and (7) were used to calculate the adsorption energy of hydrogen storage materials and the average adsorption energy data of each hydrogen molecule, as shown in Fig. 4**(a)** and 4**(b)**, respectively. Density functional methods of B3LYP and M06-2X were used to optimize the structure of the $H_2$ molecule, and the results showed that the H-H bond lengths were 0.744 Å and 0.740 Å, respectively.
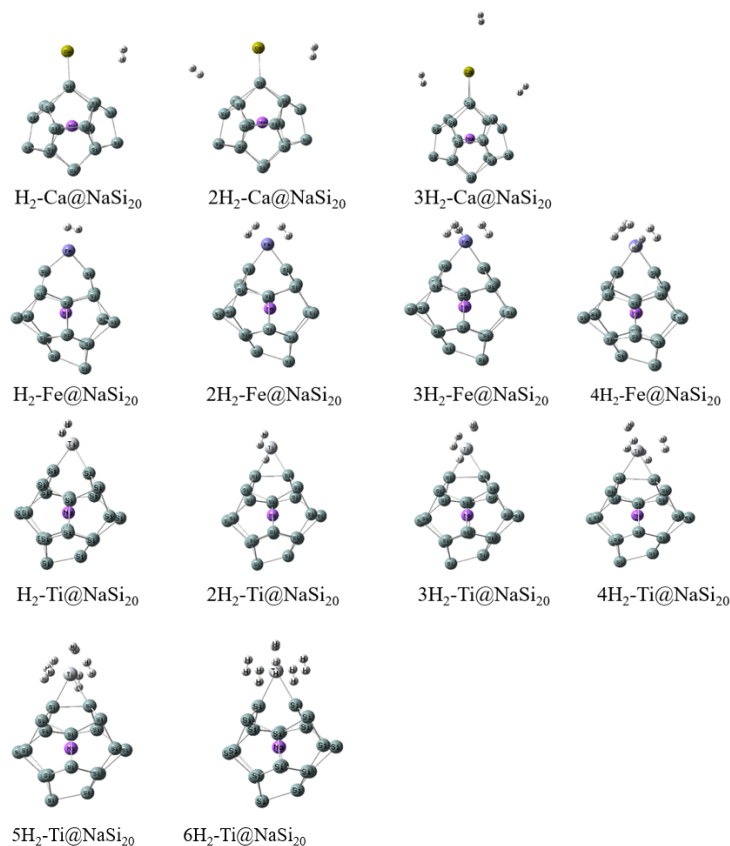


**Fig. 2.** The optimized structures for $n$H$_2$-Ca@NaSi$_{20}$, $n$H$_2$-Fe@NaSi$_{20}$ and $n$H$_2$-Ti@NaSi$_{20}$ calculated at B3LYP method.
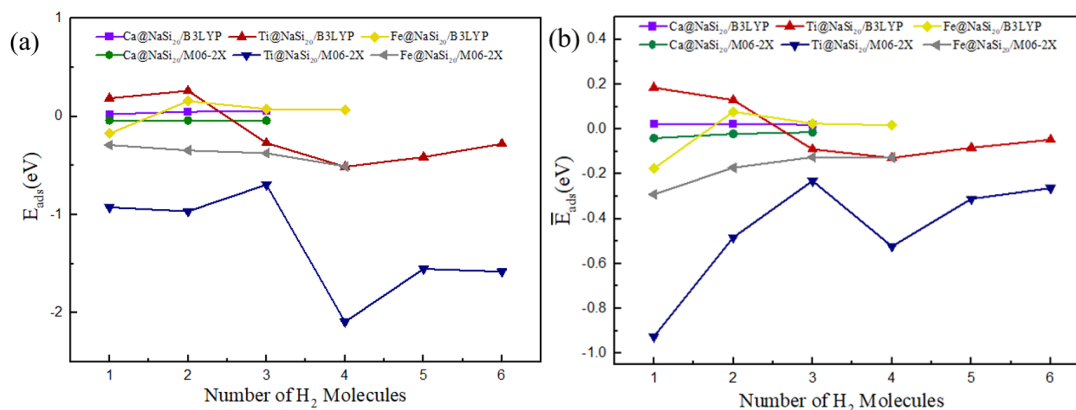


**Fig. 3. (a)** The adsorption energy ($E_{ads}$) and **(b)** the average adsorption energy per hydrogen molecule ($\bar{E}_{ads}$) for $n$H$_2$-Ca@NaSi$_{20}$, $n$H$_2$-Fe@NaSi$_{20}$ and $n$H$_2$-Ti@NaSi$_{20}$ at B3LYP and M06-2X methods.
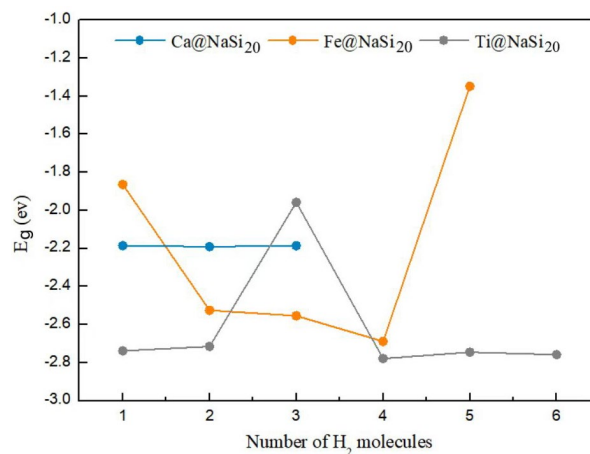
**Fig. 4.** The energy gap ($E_g$) for $n$H$_2$-Ca@NaSi$_{20}$, $n$H$_2$-Fe@NaSi$_{20}$ and $n$H$_2$-Ti@NaSi$_{20}$ at M06-2X method.

**Adsorption of H$_2$ on Ca@NaSi$_{20}$**

This section focuses on the interaction between H$_2$ and Ca@NaSi$_{20}$ clusters. As can be seen from Table 2, under the B3LYP and M06-2X methods, the interaction between a single H$_2$ molecule and the Ca@NaSi$_{20}$ cluster results in an increase of 0.023 eV and a decrease of 0.040 eV, respectively. According to Mulliken charge analysis, it can be found that the H$_2$ molecule ($Q_{H_2}$) gains a negative charge of 0.017e, the positive charge ($Q_{Ca}$) on the Ca atom decreases by 0.246e, and the charge ($Q_{Na}$) on Na atom remains basically unchanged under the B3LYP method. This indicates that there is a transfer of charge between the Ca atom and the H$_2$ molecule. The average adsorption energy of $n$H$_2$-Ca@NaSi$_{20}$ cluster is in the range of 0.019 - 0.024 eV, and the average adsorption the energy of the third H$_2$ molecule is not different from that of the second H$_2$ molecule. Under the density functional method of M06-2X, the adsorption energy ($E_{ads}$) increases from -0.040 eV to - 0.014 eV, and the absolute value of the adsorption energy ($E_{ads}$) decreases gradually when the H$_2$ molecules adsorbed by Ca@NaSi$_{20}$ cluster increase from the first H$_2$ molecule to the third H$_2$ molecule. As can be seen from Table 2, under the B3LYP method, when the second H$_2$ molecule is adsorbed by Ca@NaSi$_{20}$ cluster, the Ca-Si atomic bond length ($d_{Ca-Si}$) is 3.009 Å, and this Ca-Si atomic bond length ($d_{Ca-Si}$) is the same as the third H$_2$ adsorbed by the Ca@NaSi$_{20}$ cluster. Meanwhile, as shown in Table 2, the third H$_2$ molecule is adsorbed by the Ca@NaSi$_{20}$ cluster, the distance ($d_{Ca-H}$) between the H$_2$ molecule and the Ca@NaSi$_{20}$ cluster increases to 6.259 Å, and the H-H bond length ($d_{H-H}$) of the adsorbed third H$_2$ molecule is the same as that of a single H$_2$ molecule, both being 0.744 Å, that is, Ca@NaSi$_{20}$ cluster did not complete the adsorption of the third H$_2$ molecule. From the energy range analysis, it can also be seen from Table 2 and Fig. 4 that for the $n$H$_2$-Ca@NaSi$_{20}$ cluster, the absolute value of adsorption energy ($E_{ads}$) of the Ca@NaSi$_{20}$ cluster also increases with the increase of the H$_2$ molecule. When the Ca@NaSi$_{20}$ cluster adsorbs the third H$_2$ molecule, the absolute value of the adsorption energy ($E_{ads}$) is less than that of the second H$_2$ molecule ($E_{ads}$), which means that the third H$_2$ molecule is not adsorbed by the Ca@NaSi$_{20}$ cluster, indicating that the Ca@NaSi$_{20}$ cluster is saturated at the adsorption of the second H$_2$ molecule. Therefore, although Ca doped NaSi$_{20}$ clusters can effectively adsorb 2 H$_2$ molecules, the hydrogen storage capacity is weak, which is lower than the minimum value of reversible adsorption 0.1eV, and the system is unstable after adsorption, so it is not a relatively ideal hydrogen storage material.

**Table 2** The dipole moment (D, Debye), bond length (d, Å), adsorption energy ($E_{ads}$, eV) and Mulliken charges (Q, e) of $Ca@NaSi_{20}$.

| | D | $d_{CaSi}$ | $d_{CaH}$ | $d_{HH}$ | $E_{ads}$ | | $\bar{E}_{ads}$ | $Q_{Na}$ | | $Q_{Ca}$ | $Q_{H_2}$ |
|---|---|---|---|---|---|---|---|---|---|---|---|
| | B3LYP | B3LYP | B3LYP | B3LYP | B3LYP | M06-2X | B3LYP | M06-2X | B3LYP | B3LYP | B3LYP |
| $H_2$-Ca@NaSi$_{20}$ | 11.881 | 3.012 | 4.054 | 0.745 | 0.023 | -0.040 | 0.023 | -0.040 | -0.311 | 1.020 | -0.017 |
| $2H_2$-Ca@NaSi$_{20}$ | 11.816 | 3.009 | 4.133 | 0.745 | 0.048 | -0.041 | 0.024 | -0.021 | -0.323 | 1.029 | 0.005 |
| | | | 5.552 | 0.745 | | | | | | | -0.019 |
| $3H_2$-Ca@NaSi$_{20}$ | 11.857 | 3.009 | 4.107 | 0.745 | 0.057 | -0.042 | 0.019 | -0.014 | -0.321 | 1.030 | 0.005 |
| | | | 5.411 | 0.745 | | | | | | | -0.021 |
| | | | 6.259 | 0.744 | | | | | | | -0.001 |

## Adsorption of $H_2$ on $Fe@NaSi_{20}$

This section concerns the interaction of the $H_2$ molecules with the $Fe@NaSi_{20}$ cluster. As can be seen from Table 3, the bond length of the $H_2$ molecule increases from 0.744 Å to 0.802 Å for a single $H_2$ molecule after adsorption, increasing by 0.058 Å. After the adsorption of one $H_2$ molecule, the bond length of the Si-Fe atom ($d_{Fe-Si}$) in the $Fe@NaSi_{20}$ cluster is 2.320 Å under the B3LYP method, which is 0.047 Å shorter than the $Fe@NaSi_{20}$ cluster without adsorption of the $H_2$ molecule. The increasing of hydrogen molecular bond length ($d_{H-H}$) and the shortening of Si-Fe atom bond length ($d_{Fe-Si}$) indicate that the $H_2$ molecule is successfully adsorbed by the $Fe@NaSi_{20}$ cluster. In terms of energy range, when the number of adsorbed $H_2$ molecules increases from 1 to 4, the absolute value of adsorption energy ($E_{ads}$) calculated by the M06-2X method gradually increases from 0.291 eV to 0.508 eV, and the absolute value of average adsorption energy ($\bar{E}_{ads}$) gradually decreases from 0.291 eV to 0.127 eV. The average absolute adsorption energy of all hydrogen molecules adsorbed by clusters is greater than 0.1eV, which is within the reversible adsorption energy range of 0.1 - 0.8eV. Meanwhile, as can be seen from Fig. 5, the absolute value of the energy gap ($E_g$) increases with the increase in the number of $H_2$ molecules adsorbed by the $Fe@NaSi_{20}$ cluster. When the fourth $H_2$ molecule is adsorbed, the energy gap ($E_g$) reaches saturation. When the fifth $H_2$ molecule is adsorbed by the $Fe@NaSi_{20}$ cluster, the absolute value of the energy gap ($E_g$) becomes smaller and increases from -2.689 eV to -1.348 eV. It can be concluded that the maximum number of $H_2$ molecules adsorbed by $Fe@NaSi_{20}$ is 4. From the discussion of the energy gap, adsorption energy and average adsorption energy, it can be seen that the $Fe@NaSi_{20}$ cluster cannot effectively adsorb the fifth $H_2$ molecule. As can be seen from the Mulliken charge $Q_{Fe}$ of the Fe atom in Table 3, the negative charge density of Fe atom increases gradually during the adsorption of the $H_2$ molecule, while the charge density $Q_{Na}$ of the metal atom remains basically unchanged, and the charge density reaches saturation when the fourth $H_2$ molecule is adsorbed. Therefore, it can be seen that the $Fe@NaSi_{20}$ cluster increases the negative charge density in the outermost orbital of the Fe atom through charge transfer between the Fe atom and $H_2$ molecule in the adsorption process of $H_2$, so that Fe atom cannot store the fifth $H_2$ molecule, and the main hydrogen storage role in the system is determined by Fe atom. Therefore, Fe modified $NaSi_{20}$ cluster has strong hydrogen storage performance. Fe atoms in the $Fe@NaSi_{20}$ cluster can store up to 4 $H_2$ molecules, and the absolute value of average adsorption energy is within 0.1 - 0.8 eV. $Fe@NaSi_{20}$ cluster can realize a reversible cycle of hydrogen storage performance. Compared with the calculation results of the $Ca@NaSi_{20}$ cluster, $Fe@NaSi_{20}$ has better hydrogen storage performance.

**Table 3** The dipole moment (D, Debye), bond length (d, Å), adsorption energy ($E_{ads}$, eV) and Mulliken charges (Q, e) of $Fe@NaSi_{20}$.

| | D | $d_{Fe\text{-}Si}$ | $d_{Fe\text{-}H}$ | $d_{H\text{-}H}$ | $E_{ads}$ | | $\bar{E}_{ads}$ | | $Q_{Na}$ | $Q_{Fe}$ | $\mathbf{Q_{H_2}}$ |
|---|---|---|---|---|---|---|---|---|---|---|---|
| | **B3LYP** | **B3LYP** | **B3LYP** | **B3LYP** | **B3LYP** | **M06-2X** | **B3LYP** | **M06-2X** | **B3LYP** | **B3LYP** | **B3LYP** |
| $H_2$-$Fe@NaSi_{20}$ | 3.359 | 2.320 | 1.771 | 0.802 | -0.175 | -0.291 | -0.175 | -0.291 | -0.408 | -0.298 | 0.119 |
| $2H_2$-$Fe@NaSi_{20}$ | 3.397 | 2.260 | 1.629 | 0.851 | 0.156 | -0.345 | 0.078 | -0.172 | -0.346 | -0.434 | 0.296 |
| | | | 1.635 | 0.845 | | | | | | | 0.265 |
| $3H_2$-$Fe@NaSi_{20}$ | 3.020 | 2.275 | 1.637 | 0.838 | 0.076 | -0.374 | 0.025 | -0.125 | -0.344 | -0.614 | 0.250 |
| | | | 1.635 | 0.842 | | | | | | | 0.230 |
| | | | 1.756 | 0.796 | | | | | | | 0.126 |
| $4H_2$-$Fe@NaSi_{20}$ | 3.083 | 2.289 | 1.636 | 0.843 | 0.067 | -0.508 | 0.017 | -0.127 | -0.368 | -0.630 | 0.257 |
| | | | 1.637 | 0.839 | | | | | | | 0.255 |
| | | | 1.769 | 0.793 | | | | | | | 0.005 |
| | | | 3.387 | 0.744 | | | | | | | -0.023 |
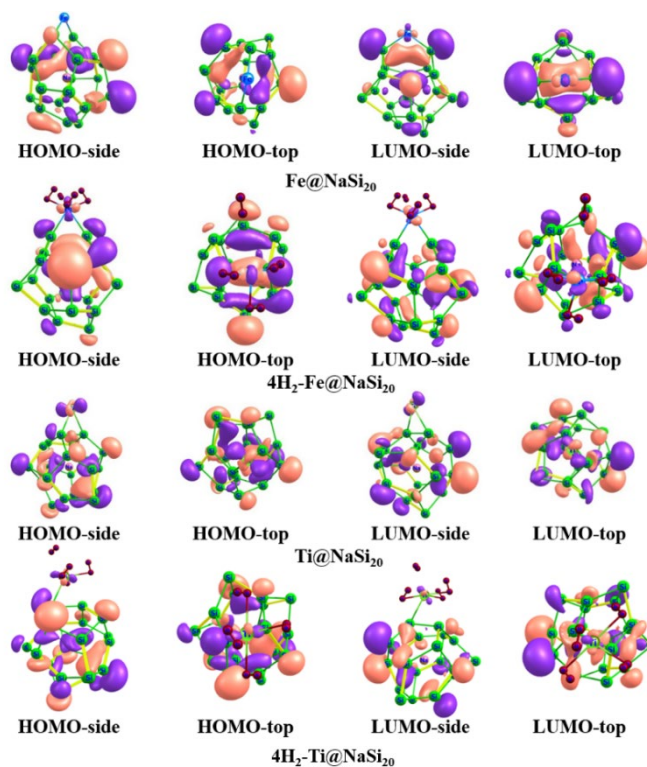


**Fig. 5.** Frontier molecular orbitals of $4H_2$-$Fe@NaSi_{20}$ (the top row) and $4H_2$-$Ti@NaSi_{20}$ (the bottom row).

### Adsorption of $H_2$ on Ti@NaSi$_{20}$

This section discusses the interaction of $H_2$ molecules with Ti@NaSi$_{20}$ clusters. Table 4 shows the geometric parameters of the optimized $nH_2$-Ti@NaSi$_{20}$(n = 6) cluster. Under the B3LYP method, the bond length ($d_{H-H}$) of the adsorbed $H_2$ molecule increases from 0.744 Å to 0.846 Å, and as can be seen from Fig. 2, there is no break in the hydrogen bond of all $H_2$ molecules adsorbed by $nH_2$-Ti@NaSi$_{20}$(n = 6) system. It indicates that $H_2$ molecules are adsorbed on the cluster in molecular form. The Ti-Si atomic bond length ($d_{Ti-Si}$) increases with the number of $H_2$ adsorbed. When the sixth hydrogen molecule is adsorbed, the maximum value of the Ti-Si atomic bond length ($d_{Ti-Si}$) is 2.656 Å. When the seventh molecule is adsorbed by the Ti@NaSi$_{20}$ cluster, the Ti-Si bond is broken. That is, the Ti-Si atomic bond length ($d_{Ti-Si}$) reaches the maximum value when the sixth $H_2$ molecule is adsorbed. Therefore, the Ti@NaSi$_{20}$ system can adsorb up to 6 $H_2$ molecules according to the bond length analysis. Under the B3LYP method, the dipole moment of the $H_2$-Ti@NaSi$_{20}$ system is 0.250 Debye smaller than that of Ti@NaSi$_{20}$, and under the M06-2X method the dipole moment of the $H_2$-Ti@NaSi$_{20}$ system is 1.022 Debye smaller than that of Ti@NaSi$_{20}$, with the decrease of dipole moment the stability of the clusters is decreased and the activity is increased. Meanwhile, Mulliken charge analysis results show that from the analysis of the charge $Q_{Ti}$ on the Ti atom, due to the charge transfer and redistribution around the metal atoms and $H_2$ molecules, compared with the Ti@NaSi$_{20}$ cluster, the positive charge of the Ti atom in $H_2$-Ti@NaSi$_{20}$ system decreases by 0.045 e, and $Q_{Ti}$ gradually decreases as the number of $H_2$ molecules adsorbs increases, and reaches the minimum value at the adsorption of the sixth $H_2$ molecule. In addition, Ti atoms have fewer electrons in their outermost shell and can accept more electrons than Fe atoms, which is one reason why Ti@NaSi$_{20}$ can attach more $H_2$ molecules than Fe@NaSi$_{20}$ clusters. The absolute values of the adsorption energy ($E_{ads}$) of the first $H_2$ molecule adsorbed by the Ti@NaSi$_{20}$ cluster were 0.185 and 0.925 eV, respectively, calculated by the B3LYP and M06-2X methods. With the number of adsorbed $H_2$ molecules gradually increasing to 6, the absolute value of adsorption energy ($E_{ads}$) first increases and then decreases, and the absolute value of average adsorption energy ($\overline{E}_{ads}$) first decreases, then increases and subsequently decreases with the increase of the adsorbed $H_2$ molecules, presenting an irregular change, which is related to the types of doped atoms and the types of atoms covered by silicon clusters [1]. But it's within the normal range. When the Ti@NaSi$_{20}$ cluster adsorbs the fourth hydrogen molecule, the absolute values of adsorption energy ($E_{ads}$) and average adsorption energy ($\overline{E}_{ads}$) reach the maximum value under the calculation of B3LYP and M06-2X, and the absolute values of adsorption energy ($E_{ads}$) are 0.512 eV and 2.091 eV, respectively. The absolute values of average adsorption energy ($\overline{E}_{ads}$) are 0.128eV and 0.523eV, respectively. In this case, the Ti@NaSi$_{20}$ cluster has the best adsorption effect on $H_2$ molecules, the system is the most stable and can realize reversible storage of $H_2$ molecules. The energy gap ($E_g$) of the system is observed to change. The energy gap ($E_g$) and mean adsorption energy ($\overline{E}_{ads}$) of the system change in the same trend, reaching the maximum value when the fourth $H_2$ molecule is adsorbed, and the value is basically unchanged when the sixth $H_2$ molecule is adsorbed. In summary, the analysis of charge density, adsorption energy, mean adsorption energy, and energy gap of the Ti@NaSi$_{20}$ cluster shows that the Ti@NaSi$_{20}$ cluster reaches the maximum value of mean adsorption energy ($\overline{E}_{ads}$) when it adsorbs 4 $H_2$ molecules, and the saturation state of $H_2$ molecular adsorption when it adsorbs 6 $H_2$ molecules. In addition, under the calculation of M06-2X, the mean adsorption energy ($\overline{E}_{ads}$) of Ti@NaSi$_{20}$ clusters for each hydrogen molecule is within the range of 0.1- 0.8 eV, which can realize reversible adsorption of hydrogen. It is also proved that Ti@NaSi$_{20}$ clusters have a better storage effect on $H_2$ molecules than Ca@NaSi$_{20}$ and Fe@NaSi$_{20}$ clusters.

**Table 4** The dipole moment (D, Debye), bond length (d, Å), adsorption energy ($E_{ads}$, eV) and Mulliken charges (Q, e) of Ti@NaSi$_{20}$.

| | D | $d_{Ti-Si}$ | $d_{Ti-H}$ | $d_{H-H}$ | $E_{ads}$ | | $\bar{E}_{ads}$ | | $Q_{Na}$ | $Q_{Ti}$ | $Q_{H_2}$ |
|---|---|---|---|---|---|---|---|---|---|---|---|
| | B3LYP | B3LYP | B3LYP | B3LYP | B3LYP | M06-2X | B3LYP | M06-2X | B3LYP | B3LYP | B3LYP |
| H$_2$-Ti@NaSi$_{20}$ | 8.252 | 2.465 | 1.957 | 0.791 | 0.185 | -0.925 | 0.185 | -0.925 | -0.344 | 0.353 | -0.155 |
| 2H$_2$-Ti@NaSi$_{20}$ | 7.850 | 2.452 | 1.870 | 0.824 | 0.261 | -0.966 | 0.130 | -0.483 | -0.347 | 0.297 | -0.131 |
| | | | 1.855 | 0.825 | | | | | | | -0.118 |
| 3H$_2$-Ti@NaSi$_{20}$ | 6.133 | 2.470 | 1.856 | 0.826 | -0.270 | -0.694 | -0.090 | -0.231 | -0.353 | 0.252 | -0.026 |
| | | | 1.855 | 0.840 | | | | | | | -0.007 |
| | | | 1.866 | 0.826 | | | | | | | 0.095 |
| 4H$_2$-Ti@NaSi$_{20}$ | 9.268 | 2.546 | 2.020 | 0.776 | -0.512 | -2.091 | -0.128 | -0.523 | -0.366 | 0.279 | -0.036 |
| | | | 2.120 | 0.768 | | | | | | | -0.054 |
| | | | 2.028 | 0.775 | | | | | | | 0.094 |
| | | | 1.980 | 0.798 | | | | | | | 0.305 |
| 5H$_2$-Ti@NaSi$_{20}$ | 6.426 | 2.535 | 1.912 | 0.814 | -0.413 | -1.552 | -0.083 | -0.311 | -0.404 | 0.220 | -0.021 |
| | | | 1.907 | 0.816 | | | | | | | 0.008 |
| | | | 2.014 | 0.793 | | | | | | | 0.101 |
| | | | 1.875 | 0.818 | | | | | | | 0.149 |
| | | | 1.844 | 0.836 | | | | | | | 0.190 |
| 6H$_2$-Ti@NaSi$_{20}$ | 7.089 | 2.656 | 1.818 | 0.846 | -0.279 | -1.580 | -0.047 | -0.263 | -0.390 | 0.240 | -0.020 |
| | | | 1.916 | 0.811 | | | | | | | 0.041 |
| | | | 1.970 | 0.803 | | | | | | | 0.103 |
| | | | 1.917 | 0.803 | | | | | | | 0.204 |
| | | | 1.995 | 0.796 | | | | | | | 0.191 |
| | | | 1.921 | 0.810 | | | | | | | 0.161 |

## Orbital analysis

The two systems with the best adsorption performance were selected for the wave function analysis. Fig. 6 shows the distribution of the highest occupied molecular orbitals (HOMO) and the lowest unoccupied molecular orbitals (LUMO) in the Fe@NaSi$_{20}$, Ti@NaSi$_{20}$, 4H$_2$-Fe@NaSi$_{20}$ and nH$_2$-Ti@NaSi$_{20}$ (n=3-6) clusters, whose analysis can be used to guide the design and characterization of novel functional hydrogen storage fullerenes. The active points are the regions of high local charge density, in which the red and green colors represent the positive and negative wave functions, respectively. As can be seen from Fig. 6, in the Fe@NaSi$_{20}$ cluster the electron cloud contribution of the Fe atoms in HOMO-LUMO is almost zero. But after the cluster adsorbed 4 H$_2$ molecules, the electron cloud around Fe atom in the 4H$_2$-Fe@NaSi$_{20}$ cluster increased

and HOMO distribution increased, which represents charge transfer between Fe atoms and $H_2$ molecules. This is consistent with the previous charge analysis of $Q_{Fe}$ and $Q_{H_2}$. For the $Ti@NaSi_{20}$ cluster, HOMO and LUMO are partially distributed on Ti and partially distributed on the $NaSi_{20}$ cluster when there is no $H_2$ molecule adsorbed. With the increase of $H_2$ molecules from 3 to 6, the distribution of frontier orbitals on Ti gradually decreases. When four $H_2$ molecules are adsorbed, there are a few unoccupied orbitals around Ti atoms, indicating that they can still adsorb $H_2$ molecules, which is consistent with the previous analysis trend.
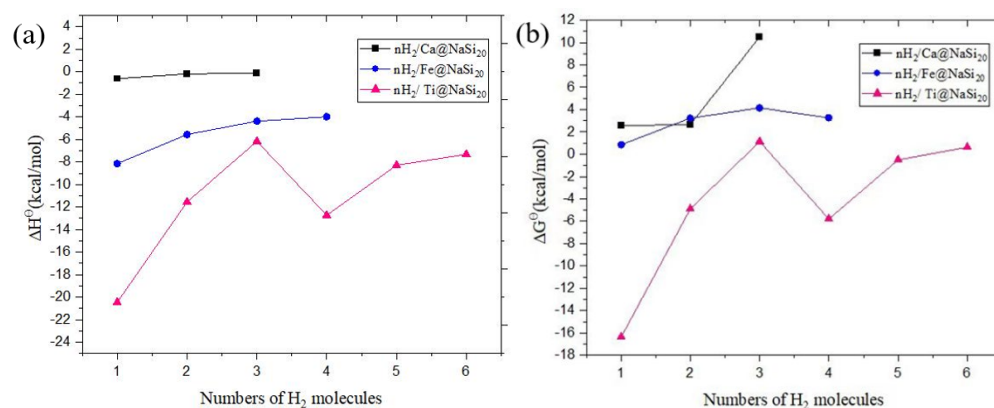


**Fig. 6. (a)** Enthalpy difference ($\Delta H^{\ominus}$) and **(b)** free energy difference ($\Delta G^{\ominus}$) for $nH_2/Ca@NaSi_{20}$, $nH_2/Fe@NaSi_{20}$ and $nH_2/Ti@NaSi_{20}$ calculated at M06-2X method.

**Adsorbed $H_2$ prediction**

Theoretically, the Effective Atomic Number Rule (EAN) can be used to calculate the maximum adsorption capacity of hydrogen atoms of hydrogen storage material with surface doped metal atoms [26]. The equation is as follows,

$$n_H = 18 - n_v^e - n_s^e - n_m^e \qquad (10)$$

where $n_v^e$ is the number of valence electrons of the metal atom, $n_s^e$ is the bonding number of the metal to the substrate, and $n_m^e$ is the bonding number between neighboring metal atoms. Considering the 3d orbitals of transition metal atoms Ti and Fe, the valence electron numbers ($n_v^e$) of Ca, Fe, and Ti atoms are 2, 8, and 4, respectively. Since M is adsorbed above the Si-Si bond, $n_s^e = 2$, the $n_H$ of $M@NaSi_{20}$ (M = Ca, Fe, and Ti) is calculated to be 14, 8, and 12, respectively, which means that the maximum adsorption numbers of hydrogen molecules are 7, 4, and 6. Compared with the calculated results, it can be seen that the hydrogen storage performance of $Ca@NaSi_{20}$ is less than the theoretical results, so the hydrogen storage performance is poor. The maximum hydrogen storage number of $M@NaSi_{20}$ (M = Fe and Ti) is in accordance with the theoretical expectation, *i.e.*, the number of $H_2$ molecules that can be adsorbed is in accordance with EAN. At the same time, we tried to adsorb the third, 5th, and 7th $H_2$ molecules on $Ca@NaSi_{20}$, $Fe@NaSi_{20}$, and $Ti@NaSi_{20}$, respectively. None of the results calculated by the density functional method can converge, which further indicates that $Ca@NaSi_{20}$, $Fe@NaSi_{20}$, and $Ti@NaSi_{20}$ can adsorb at most 2, 4, and 6 $H_2$ molecules.

**Thermodynamic analysis**

The enthalpy difference ($\Delta H^{\ominus}$) can express the strength of the interaction and the free energy difference ($\Delta G^{\ominus}$) is a measure of the spontaneity of the reaction, which are the key thermodynamic parameters for the interaction between hydrogen and the sorbent materials. $\Delta H^{\ominus}$ and $\Delta G^{\ominus}$ are graphed in Fig. 7 as a function of the number of hydrogen molecules for $nH_2$-$Ca@NaSi_{20}$, $nH_2$-$Fe@NaSi_{20}$, and $nH_2$-$Ti@NaSi_{20}$ complexes. As

shown in Fig. 7a, $\Delta H^{\ominus}$ values are negative for all the considered structures, indicating exothermic reactions. For all the complexes of the $n$H$_2$-Ti@NaSi$_{20}$ system only the free energy difference of 1H$_2$-Ti@NaSi$_{20}$, 2H$_2$-Ti@NaSi$_{20}$, 4H$_2$-Ti@NaSi$_{20}$, 5H$_2$-Ti@NaSi$_{20}$ is negative ($\Delta G^{\ominus} < 0$), which shows that they are spontaneous reactions. In the $n$H$_2$-Ti@NaSi$_{20}$ system, when n = 1 the absolute value of $\Delta H^{\ominus}$ decreases as the number of H$_2$ molecules increases, and the absolute value of $\Delta H^{\ominus}$ is 20.45 kcal/mol. It can be seen from Fig. 7b, in all the complexes, 3H$_2$-Ca@NaSi$_{20}$ has the largest value of free energy difference ($\Delta G^{\ominus}$), which is 10.50 kcal/mol. As a negative $\Delta H^{\ominus}$ value indicates stronger stability, and a negative $\Delta G^{\ominus}$ value indicates stronger reversal ability of the reaction, with the increase of the number of hydrogen molecules, the stability decreases, the hydrogen storage capacity gradually reaches saturation, and the desorption ability of H$_2$ molecules increases [27-29].

## Conclusions

In this work, the storage characteristics of H$_2$ molecules on NaSi$_{20}$ fullerenes deposited by Ca, Fe, and Ti were investigated at the theoretical level of the DFT-based B3LYP and M06-2X methods. The results show that the encapsulated Na atom into the Si$_{20}$ cluster delivers the regular shape to the NaSi$_{20}$. The deposition of the Ca, Fe and Ti atoms on NaSi$_{20}$ clusters decreases the ionization potential (IP), HOMO-LUMO energy gap ($E_g$), and hardness ($\eta$), and increases the dipole moment (D), which confirms that Ca@NaSi$_{20}$, Fe@NaSi$_{20}$, and Ti@NaSi$_{20}$ clusters are less stable and therefore more reactive than NaSi$_{20}$ clusters.

Additionally, the Ca@NaSi$_{20}$, Fe@NaSi$_{20}$, and Ti@NaSi$_{20}$ clusters are saturated by two, four, and six H$_2$ molecules, respectively. The adsorption energy values ($E_{ads}$) per hydrogen molecule meet the U. S. DOE target for hydrogen storage materials for $n$H$_2$-Ti@NaSi$_{20}$ ($n$ = 2 - 6) and $n$H$_2$-Fe@NaSi$_{20}$ ($n$ = 1-4), which implies that NaSi$_{20}$ fullerenes may be a potentially suitable material for hydrogen storage. The calculated enthalpy differences emphasize that some hydrogen molecules are physisorbed on the studied clusters with an effect greater than one.

## Acknowledgements

## References

1. Hoel, M.; Kverndok, K. *Resour Energy Econ.* **1996**, 18, 115-136.
2. Kale, P. *Int J Hydrogen Energy.* **2012**, 37, 3741-3747.
3. Bailleux, C. *Int J Hydrogen Energy.* **1981**, 6, 461.
4. Mazloomi, K. *Renew Sust Energ Rev.* **2012**, 16, 3024-3033.
5. Anafcheh, M. *Int J Hydrogen Energy.* **2018**, 43, 12271-12277.
6. Xu, W. *Prog Chem.* **2006**, 18, 200-201.
7. Gong, J. M. *Natural Gas Chem. Indus.* **2010**, 5, 71.
8. Sahaym, U. *J Mater Sci.* **2008**, 43, 5395.
9. Wang, Q.; Sun, Q.; Jena, P.; Kawazoe, Y. *J Chem Theory Comput.* **2009**, 5, 374-379.
10. Zhang, D. J.; Ma, C.; Liu, C. B. *J Phys Chem C.* **2007**, 111, 17099.
11. Khanna, S. N.; Rao, B. K.; Jena, P. *Phys Rev Lett.* **2002**, 89, 016803.

12. Kumar, V.; Kawazoe, Y. *Phys Rev Lett.* **2003**, 90, 055502.
13. Ryou, J.; Hong, S.; Kim, G. *Solid State Commun*. **2008**, 148, 469-471.
14. Kumar, V.; Kawazoe, Y. *Phys Rev B*. **2007**, 75, 155425.
15. Sporea, C.; Rabilloud, F. *J Chem Phys*. **2007**, 127, 164306.
16. Ammar, H. Y.; Badran, H. M. *Int J Hydrogen. Energy.* **2021**, 46, 14565-14580.
17. Williamson, A. J.; Reboredo, F. A.; Galli, G. *Appl Phys Lett*. **2004**, 85, 2917-2919.
18. Yoon, M.; Yang, S.Y.; Hicke, C.; Wang, E. *Phys Rev Lett.* **2008**, 100, 206806.
19. Wang, C. J.; Tang, C. M.; Zhang, Y. J.; Gao, F. Z. *Chem Res Chin Univ*. **2014**, 35, 2131-2137.
20. Kohn, W.; Sham, L. J. *Phys Rev*. **1965**, 140, 1133-1138.
21. Mao, W. L.; Mao, H. K. *Proc Natl Acad Sci USA*. **2004**, 101, 708-710.
22. Frisch, M. J. Gaussian 09, revision D.01, *Wallingford, CT: Gaussian, Inc*, *2009*.
23. Guo, C.; Wang, C. *Int J Hydrogen Energy*. **2019**, 44, 10763-10769.
24. Borshch, N. A.; Pereslavtseva, N. S.; Kurganskiĭ, S. I. *Semiconductors.* **2006**, 40, 1457-1462.
25. Baei, M. T.; Koohi, M.; Shariati, M. *J Mol Struct.* **2018**, 1159, 118-134.
26. Kubas, G. J. *Kluwer Academic/Plenum Publishing. 2001*.
27. Padhee, S. P.; Roy, A.; Pati, S. *Int J Hydrogen Energy.* **2021**, 46, 906-921.
28. Liu, Z. C.; Ruan, Y. M.; Li, F.; Zhang, G. F.; Zhao, M. *Int J Hydrogen Energy.* **2021**, 46, 4201-4210.
29. Pluengphon, P.; Tsuppayakorn-aek, P.; Inceesungvorn, B. *Int J Hydrogen Energy.* **2020***, 45, 25065-25074.